

Supporting Information
Factor Analysis of Conformations and NMR Signals of Rotaxanes:
AIMD and Polarizable MD Simulations

Pingying Liu^{1,2}, Wei Li^{*1}, Zigui Kan¹, Hui Sun¹, Jing Ma^{*1}

¹School of Chemistry and Chemical Engineering, Key Laboratory of Mesoscopic Chemistry of MOE, Nanjing University, Nanjing 210093, People's Republic of China

²School of Materials Science and Engineering, Jingdezhen Ceramic Institute, Jingdezhen 333403, China

*Corresponding author: majing@nju.edu.cn, Fax: 86-25-83686131, Tel: 86-25-89687408

*Corresponding author: wli@nju.edu.cn, Tel: 86-25-89687052

Contents

1. Figure S1. (a) Convergence behaviors of calculated ¹ H chemical shifts of amide protons for the pseudorotaxane in vacuum. (b) Structural variations with the time evolutions.	S2
2. Figure S2. Comparison of PW91-based AIMD with the GEBF-M06-2X AIMD and the force field based MD simulations.	S3
3. Figure S3. Flow chat of polar-FF MD simulations.	S4
4. Figure S4. Potential energies varied as a function of time for the pseudorotaxane.	S5
5. Table S1. Correlation matrix of PC-FA method.	S6
6. Table S2. Total variance explained result of PC-FA method.	S6
7. Table S3. Component score coefficient matrix of PC-FA method.	S6
8. Figure S5. Comparison of the number of H-bonds as a function of MD simulation time using four different molecular dynamics methods for pseudorotaxane in vacuum.	S7
9. Figure S6. The first principle component scores of ring-rod contacting geometries for pseudorotaxane in vacuum using polar FF+AIMD method.	S8
10. Figure S7. Fluctuations of end-to-end lengths of rod for the pseudorotaxane using non-polar and polar FF MD simulations in vacuum and in solution.	S9
11. Figure S8. Variation of number of solvents around the solute using (a) non-polar FF and (b) polar FF-based MD simulations in solution for [2]rotaxane.	S10
12. Figure S9. Distributions of N···O lengths and N-H···O angles for pseudorotaxane in vacuum and in solution.	S11
13. Figure S10. PC1 score plots for (a) pseudorotaxane, and (b) [2]rotaxane using non-polar and polar FF MD simulations in vacuum and in solution.	S12

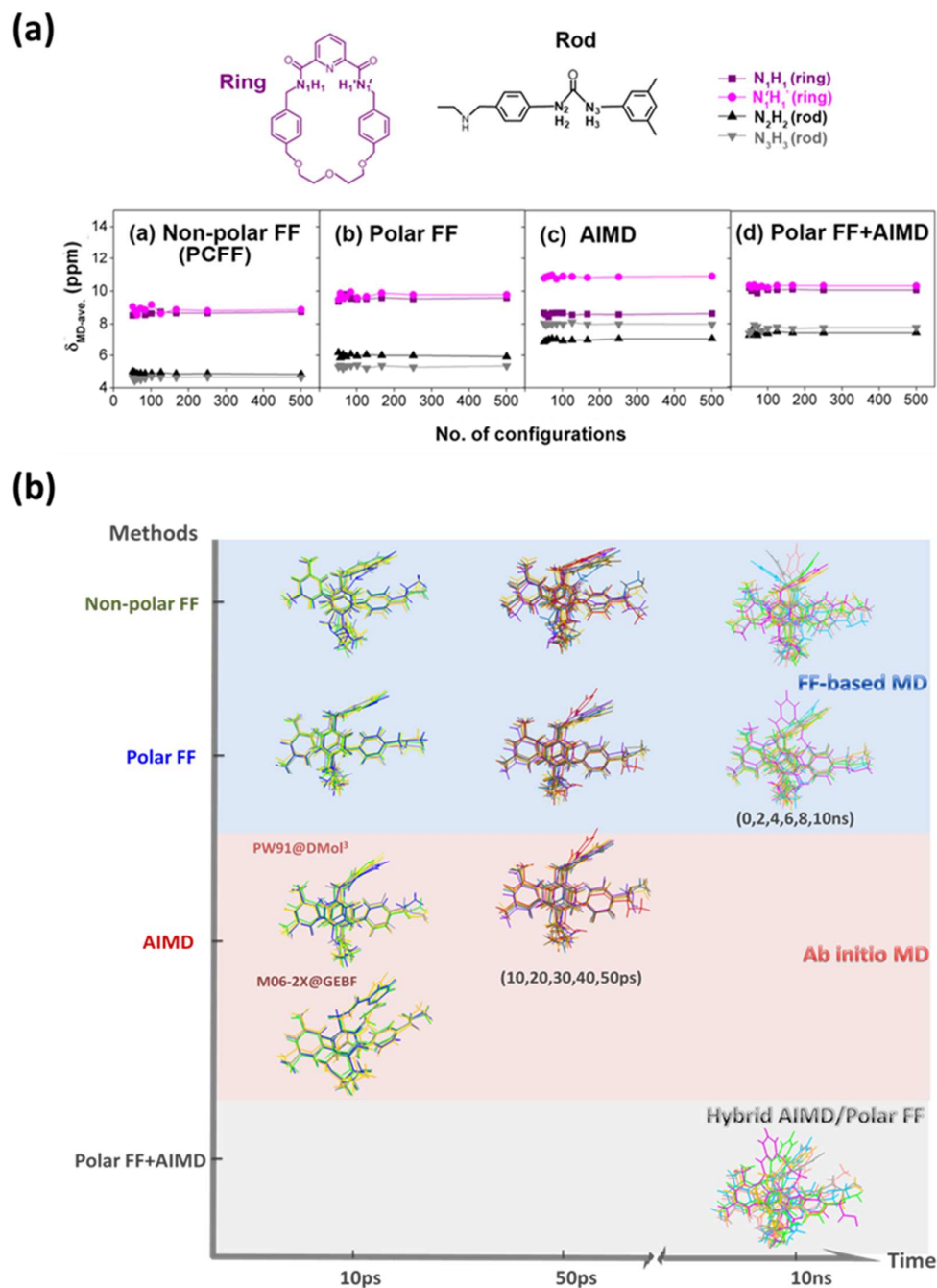


Figure S1. (a) Convergence behaviors of calculated ^1H chemical shifts of amide protons for the pseudorotaxane in vacuum. (b) Structural variations with the time evolutions.

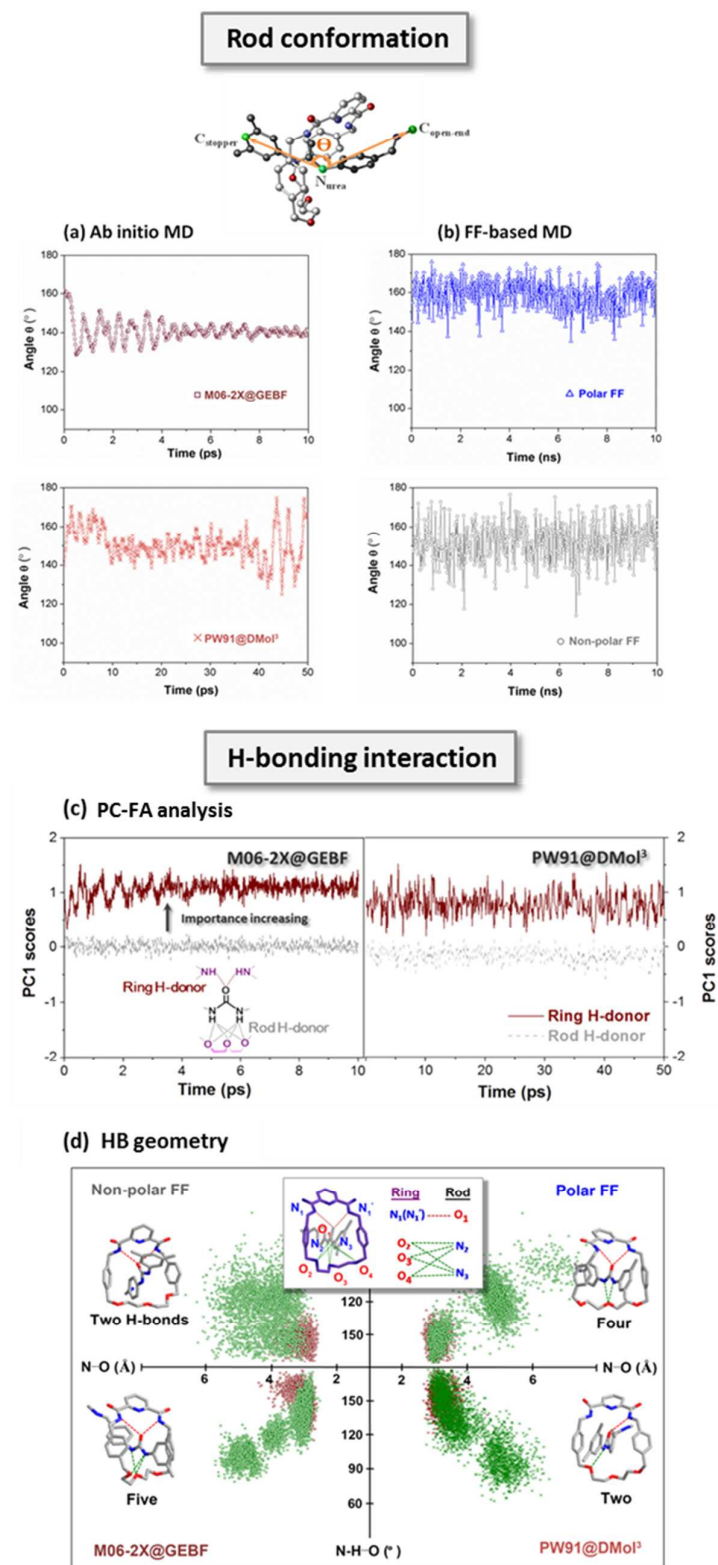


Figure S2. The comparison of PW91-based AIMD with the GEBF-M06-2X AIMD and the force field based MD simulations.

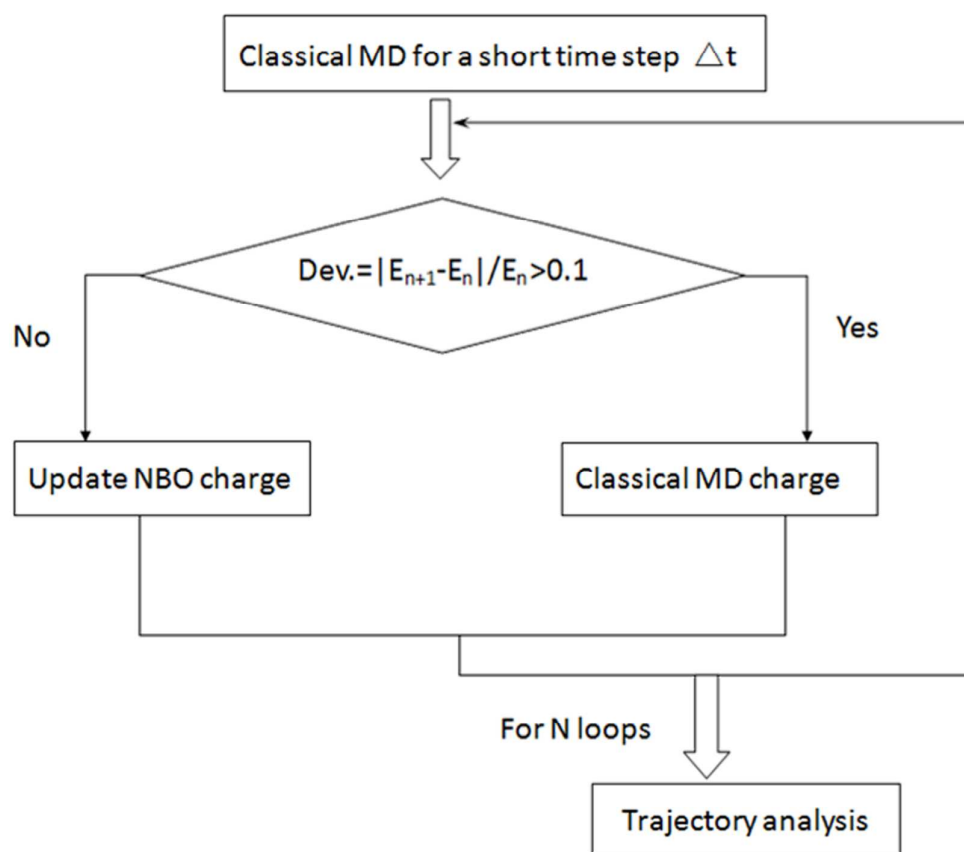


Figure S3. Flow chart of polar-FF MD simulations.

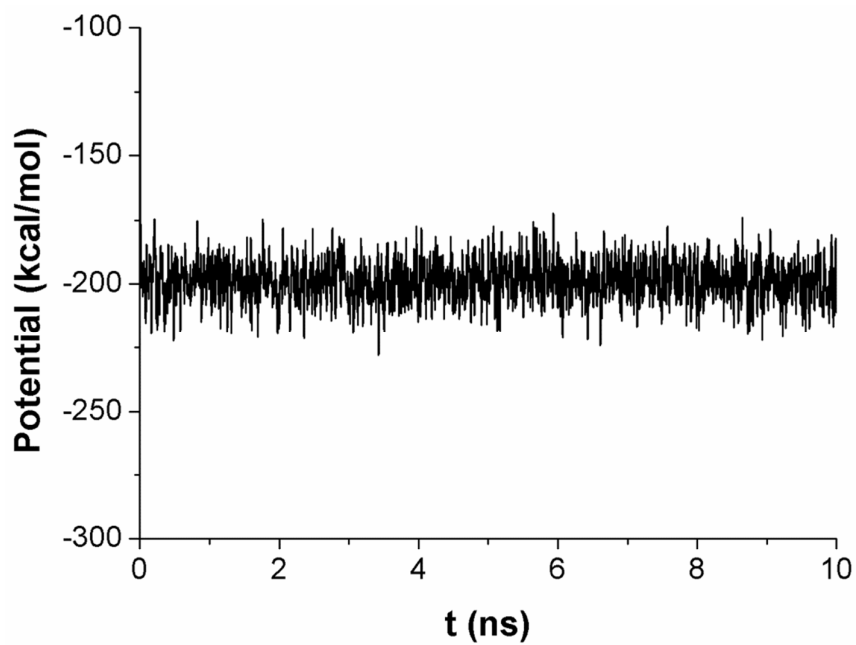


Figure S4. Potential energies (kcal/mol) varied as a function of time for the pseudorotaxane. The molecular dynamics simulation are carried out at 298.15K by using PCFF with NBO charges, updated every 5ps.

Table S1. Correlation matrix of factor analysis using principal component method.

	$\angle\text{N-H}\cdots\text{O}$	$r_{\text{N}\cdots\text{O}}$	$r_{\text{N-H stretch}}$	$r_{\text{H}\cdots\text{O}}$	$r_{\text{N-H}} / r_{\text{H}\cdots\text{O}}$
$\angle\text{N-H}\cdots\text{O}$	1.000	-0.656	0.037	-0.752	0.711
$r_{\text{N}\cdots\text{O}}$	-0.656	1.000	-0.170	0.971	-0.930
$r_{\text{N-H stretch}}$	0.037	-0.170	1.000	-0.172	0.291
$r_{\text{H}\cdots\text{O}}$	-0.752	0.971	-0.172	1.000	-0.948
$r_{\text{N-H}} / r_{\text{H}\cdots\text{O}}$	0.711	-0.930	0.291	-0.948	1.000

Table S2. Total variance explained result of factor analysis using principal component method.

Component	Initial eigenvalues			Extraction Sums of Squared Loadings		
	Total	% of Variance	Cumulative %	Total	% of Variance	Cumulative %
1	3.546	70.916	70.916	3.546	70.916	70.916
2	0.991	7.700	90.735			
3	0.385	1.191	98.434			
4	0.060	0.375	9.625			
5	0.019	0.018	100.000			

Table S3. Component score coefficient matrix of factor analysis using principal component method.

	Principal Component 1
$\angle\text{N-H}\cdots\text{O}$	0.229
$r_{\text{N}\cdots\text{O}}$	-0.270
$r_{\text{N-H stretch}}$	0.071
$r_{\text{H}\cdots\text{O}}$	-0.277
$r_{\text{N-H}} / r_{\text{H}\cdots\text{O}}$	0.274

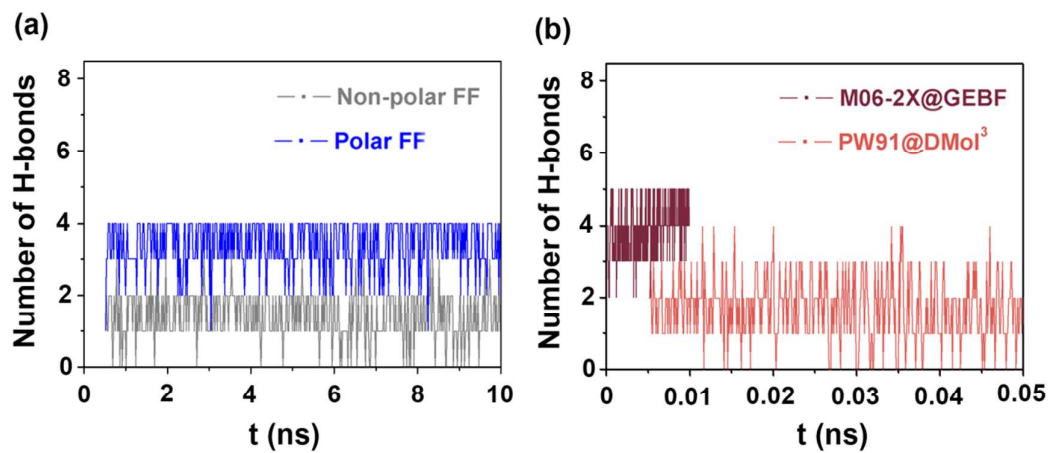


Figure S5. Comparison of the number of H-bonds as a function of MD simulation time using four different molecular dynamics methods for pseudorotaxane in vacuum.

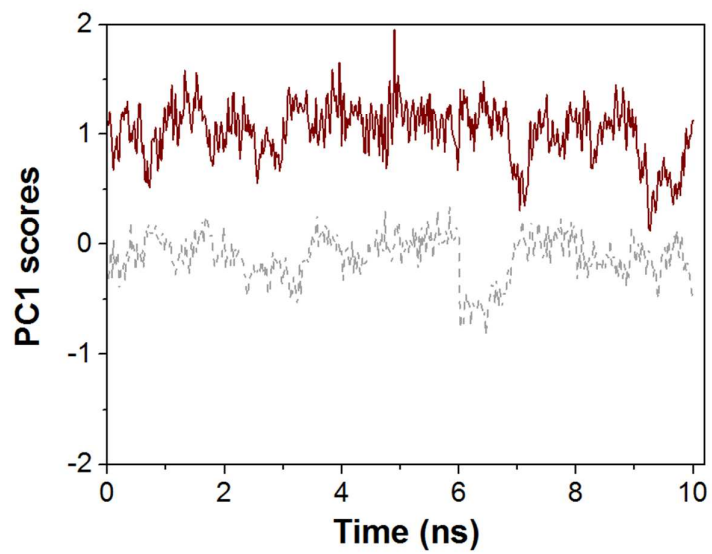


Figure S6. The first principle component scores of ring-rod contacting geometries for pseudorotaxane in vacuum using polar FF+AIMD method.

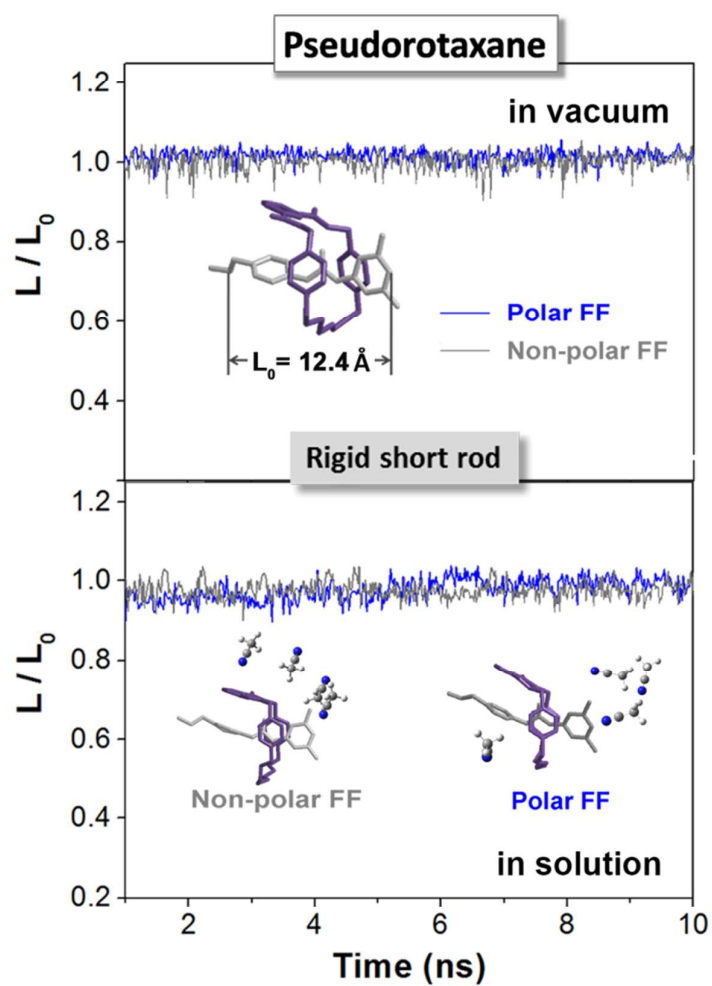


Figure S7. Fluctuations of end-to-end lengths of rod for pseudorotaxane using non-polar and polar FF MD simulations in vacuum and in solution.

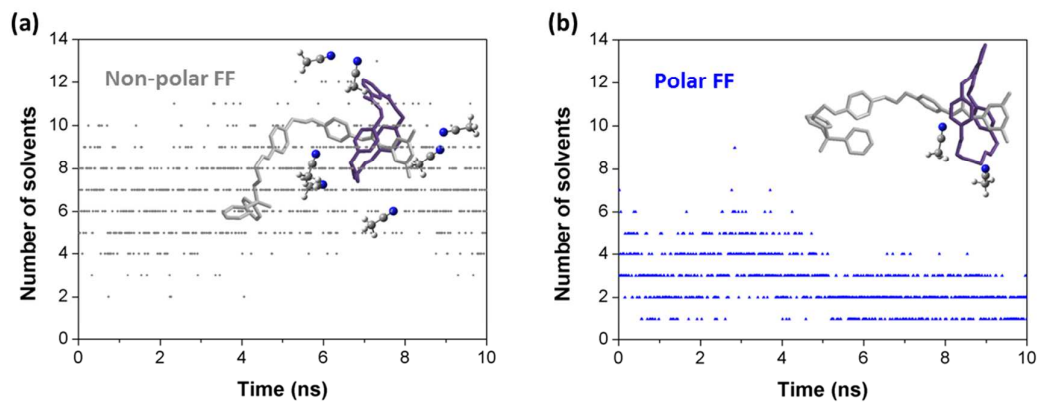


Figure S8. Variation of number of solvents around the solute with the distance cutoff ($< 9 \text{ \AA}$) using (a) non-polar FF and (b) polar FF-based MD simulations in solution for [2]rotaxane.

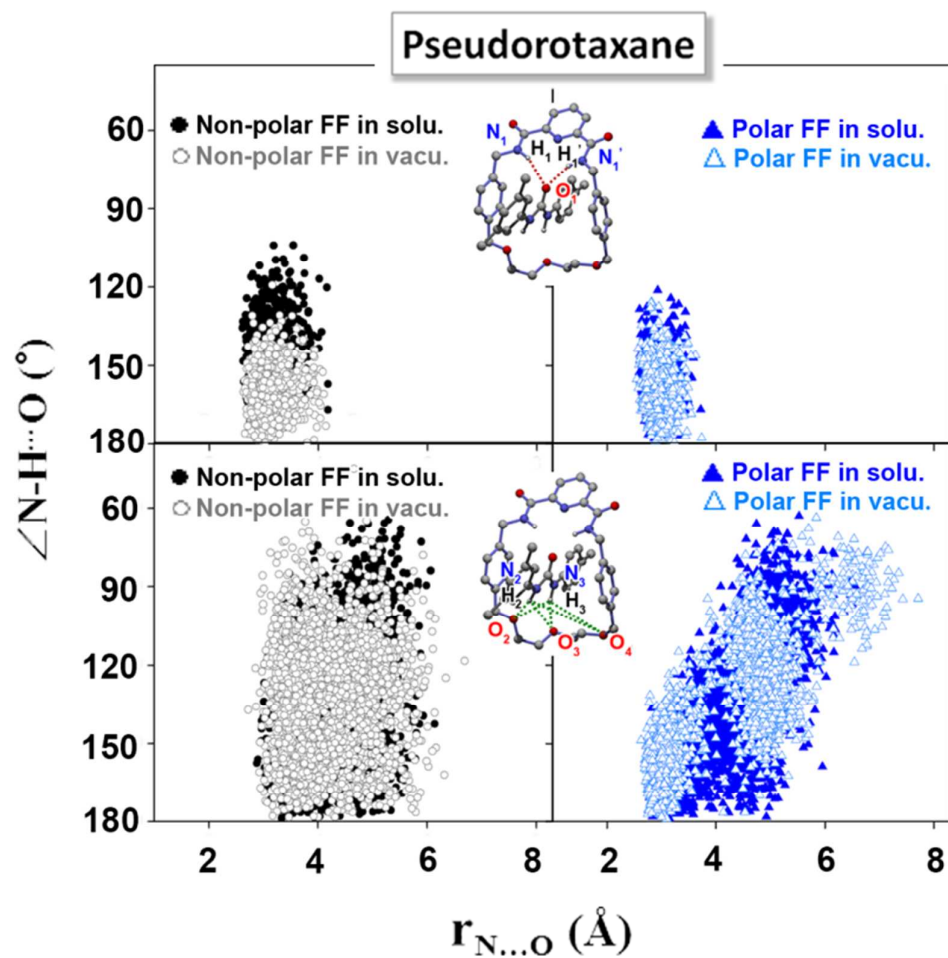


Figure S9. Distributions of $N...O$ lengths and $N-H...O$ angles for pseudorotaxane in vacuum and in solution.

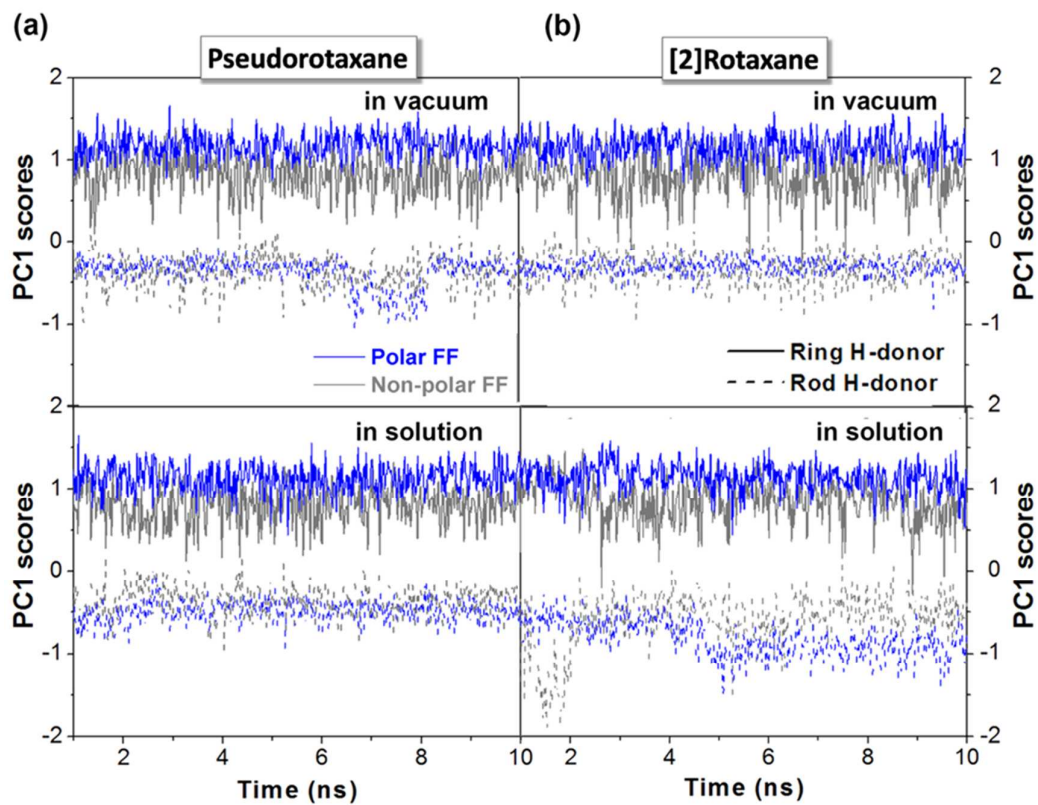


Figure S10. PC1 score plots for (a) pseudorotaxane, and (b) [2]rotaxane using non-polar and polar FF MD simulations in vacuum and in solution.